Monthly Notices of the ROYAL ASTRONOMICAL SOCIETY

MNRAS **529,** 1019–1034 (2024) https://doi.org/10.1093/mnras/stae124
Advance Access publication 2024 March 9

# High energy gamma-ray sources in the VVV survey - II. The AGN counterparts

Laura G. Donoso ,[1★] Ana Pichel,[2] Laura D. Baravalle,[3,4★] M. Victoria Alonso,[3,4★] Eduardo O. Schmidt,[3,4] Dante Minniti,[5,6,7] Nicola Masetti,[5,8] Leigh C. Smith,[9] Philip W. Lucas ,[10] Carolina Villalon ,[3] Adrián C. Rovero[2] and Georgina Coldwell [11]

[1]*Instituto de Ciencias Astronómicas, de la Tierra y del Espacio (ICATE, CONICET), C.C. 467, 5400, San Juan, Argentina*
[2]*Instituto de Astronomía y Física del Espacio (IAFE, CONICET-UBA), C1428ZAA, Ciudad Autónoma de Buenos Aires, Argentina*
[3]*Instituto de Astronomía Teórica y Experimental (IATE, CONICET-UNC), Laprida 854, X5000, Córdoba, Argentina*
[4]*Observatorio Astronómico de Córdoba, Universidad Nacional de Córdoba, X5000BGR, Córdoba, Argentina*
[5]*Instituto de Astrofísica, Facultad de Ciencias Exactas, Universidad Andrés Bello, Av. Fernandez Concha 700, Las Condes, Santiago, 7591538 Chile*
[6]*Vatican Observatory, V-00120 Vatican City, Vatican City State*
[7]*Departamento de Física, Universidade Federal de Santa Catarina, Trinidade, 88040-900 Florianopolis, Brazil*
[8]*INAF - Osservatorio di Astrofisica e Scienza dello Spazio, via Piero Gobetti 101, I-40129 Bologna, Italy*
[9]*Institute of Astronomy, University of Cambridge, Madingley Road, Cambridge CB3 0HA, UK*
[10]*Centre for Astrophysics, University of Hertfordshire, College Lane, Hatfield AL10 9AB, UK*
[11]*Departamento de Geofísica y Astronomía, Facultad de Ciencias Exactas, Físicas y Naturales , (CONICET-UNSJ), J5402DCS San Juan, Argentina*

Accepted 2024 January 8. Received 2023 December 18; in original form 2023 September 30

## ABSTRACT

We identified Active Galactic Nuclei (AGN) candidates as counterparts to unidentified gamma-ray sources (UGS) from the *Fermi*-LAT Fourth Source Catalogue at lower Galactic latitudes. Our methodology is based on the use of near- and mid-infrared photometric data from the VISTA Variables in the Vía Láctea (VVV) and Wide-field Infrared Survey Explorer (WISE) surveys. The AGN candidates associated with the UGS occupy very different regions from the stars and extragalactic sources in the colour space defined by the VVV and WISE infrared colours. We found 27 near-infrared AGN candidates possibly associated with 14 *Fermi*-LAT sources using the VVV survey. We also found 2 blazar candidates in the regions of 2 *Fermi*-LAT sources using WISE data. There is no match between VVV and WISE candidates. We have also examined the $K_s$ light curves of the VVV candidates and applied the fractional variability amplitude ($\sigma_{rms}$) and the slope of variation in the $K_s$ passband to characterise the near-infrared variability. This analysis shows that more than 85 per cent of the candidates have slopes in the $K_s$ passband $>10^{-4}$ mag/day and present $\sigma_{rms}$ values consistent with a moderate variability. This is in good agreement with typical results seen from type-1 AGN. The combination of $YJHK_s$ colours and $K_s$ variability criteria was useful for AGN selection, including its use in identifying counterparts to *Fermi* $\gamma$-ray sources.

**Key words:** galaxies: active – infrared: galaxies – surveys – catalogues.

## 1 INTRODUCTION

Since its launch in June 2008, the *Fermi* Large Area Telescope (Atwood 2009, *Fermi*-LAT) has revolutionised our view of the $\gamma$-ray sky above 100 MeV. The *Fermi*-LAT offers a significant increase in sensitivity, improved angular resolution, and nearly uniform sky coverage, making it a powerful tool for the detection and characterisation of large numbers of $\gamma$-ray sources. The *Fermi* Fourth Source Catalogue (Abdollahi et al. 2020, 4FGL), based on the first 8 yr of data from the mission, lists 5064 sources in the energy range 50 MeV–1 TeV. Out of these sources, 1336 (26.4 per cent) sources do not have even a reliable association with sources detected at other wavelengths; we will henceforth label them as Unassociated Gamma-ray Sources (UGS). More than 3130 of the identified or associated sources are active galaxies of the blazar class, and 239 are pulsars.

The positions of $\gamma$-ray sources listed in the *Fermi*-LAT catalogues are reported with their associated uncertainty represented by an elliptical region. The *Fermi*-LAT $\gamma$-ray catalogues provide the semimajor and semiminor axes of the ellipses together with the positional angle at 68 per cent and 95 per cent level of confidence. The principal reason for the difficulty of finding counterparts to high-energy $\gamma$-ray sources has been the large positional errors in their measured locations, a result of the limited photon statistics and angular resolution of the $\gamma$-ray observations and the bright diffuse $\gamma$-ray emission from the Milky Way (MW). Therefore, the UGS represent one of the biggest challenges in $\gamma$-ray astrophysics (e.g. Thompson 2008). The key to finding plausible counterparts to the unidentified *Fermi*-LAT sources is the cross-check with observations at one or more wavelengths, such as radio observations (e.g. Hovatta et al. 2014; Schinzel et al. 2015), infrared observations (e.g. Raiteri et al. 2014) and in the

★ E-mail: lauradsj@gmail.com (LGD); laurabaravalle@gmail.com (LB); m.v.alonso@gmail.com(MVA)

sub-millimetre range (e.g. León-Tavares et al. 2012; López-Caniego et al. 2013). Additional X-ray studies have also been carried out with *Chandra* and *Suzaku* have been useful in particular when performed in the crowded region of the Galactic plane (e.g. Maeda et al. 2011; Cheung et al. 2012). Optical spectroscopic identification of *Fermi* sources has been addressed previously to search for counterparts (e.g. Paggi et al. 2014; Peña-Herazo et al. 2021; García-Pérez et al. 2023). In addition, the properties of the $\gamma$-ray sources can be used as a statistical set to perform a multivariate analysis. This is a classification strategy to find plausible counterparts at other wavelengths for sources that remain unassociated (e.g. Hassan et al. 2013; Doert & Errando 2014).

Active Galactic Nuclei (AGN) represent an astronomical phenomenon that emit extremely high-energy radiation, as demonstrated by Urry & Padovani (1995) and Padovani et al. (2017). Since their discovery many decades ago, research has been conducted at various frequencies unveiling the diverse manifestations of AGN phenomena, observed from radio to $\gamma$-rays. This has resulted in an extensive and captivating assortment of classifications. Among the distinct classes of AGN are type-1 and type-2 AGN, blazars sub-divided in BL Lacertae and Flat Spectrum Radio Quasars (FSRQ), alongside other classifications (see, Stickel et al. 1991; Stocke et al. 1991). The AGN unification scheme, as proposed by Antonucci (1993), offers a comprehensive representation of AGN phenomena, including elements such as black holes, discs, torus, clouds, and jets. This model explains how orientation effects, different accretion powers, and black hole spin parameters can account for the wide array of AGN types. Furthermore, AGN typically exhibit variations in their emissions (Edelson et al. 2002; Sandrinelli, Covino & Treves 2014; Husemann et al. 2022). The extent of this variability differs according to the type of AGN and is generally more pronounced, with higher amplitudes in blazars compared to type-1 AGN (e.g. Ulrich, Maraschi & Urry 1997; Mao & Yi 2021; Baravalle et al. 2023).

In recent years, the population of known AGN has substantially grown thanks to new surveys and catalogues (e.g. Véron-Cetty & Véron 2010; Rembold et al. 2017; do Nascimento et al. 2019). Nevertheless, the number of AGN observed at lower Galactic latitudes, obscured by dense regions belonging to our Galaxy, remains limited (e.g. Edelson & Malkan 2012; Pichel et al. 2020). Recently, Fu et al. (2021, 2022) explored the Galactic bulge regions in search for quasars (QSO) at lower latitudes. Employing machine learning techniques, they identified and confirmed 204 QSO candidates at ($|b| < 20°$) based on spectroscopic measurements. Ackermann et al. (2012) reported a significant excess of unassociated sources at $|b| < 10°$, where catalogues of AGN are incomplete. Hence the fraction of sources associated with AGN decreases in this sky area.

Extragalactic objects located behind the MW are difficult to identify and detect due to the significant amount of gas, dust, and stars present at low Galactic latitudes (e.g. Kraan-Korteweg 2000; Baravalle et al. 2018, 2021). In this context, observations carried out at near-infrared wavelengths minimize the effects of interstellar extinction in these regions in comparison with optical passbands. Although the density of foreground sources is greater in the near-infrared, the reduced foreground extinction can reveal different physical processes. Studying these unknown MW regions at low Galactic latitudes, which are usually obscured at visible wavelengths, presents a challenging task. The first near-infrared survey in these regions was the Two Micron All Sky Survey (Skrutskie et al. 2006, 2MASS). Later, the ESO Public Surveys, the VISTA Variables in the Vía Láctea (Minniti et al. 2010, VVV) and its extension, the VVVX have been mapping the $K_s$-passband variability of stars in the entire MW bulge and disc. The main scientific goal was to gain more insight into the inner MW's origin, structure, and evolution. The VVV survey included the acquisition of $ZYJHK_s$ images whereas VVVX was restricted to the $JHK_s$ passbands, increasing significantly the coverage area (see table 1 in Daza-Perilla et al. 2023). Thousands of new galaxies and galaxy associations have been discovered using the photometric data from VVV and VVVX surveys (e.g. Amôres et al. 2012; Coldwell et al. 2014; Baravalle et al. 2019; Galdeano et al. 2021; Soto et al. 2022; Daza-Perilla et al. 2023). The VVV near-infrared galaxy catalogue (Baravalle et al. 2021, VVV NIRGC) is the final catalogue of part of the Southern Galactic disc using the colour criteria and the visual inspection to identify 5554 galaxies. Only 45 of these galaxies were previously known. Pichel et al. (2020) studied for the first time the active galaxies in these regions using a combination of near-infrared (NIR) and mid-infrared (MIR) data. The *Wide-field Infrared Survey Explorer* (Wright et al. 2010, WISE) is an ideal mission for identifying a very large number of AGN across the full sky. Additionally, Baravalle et al. (2023) reported four AGN candidates at very low Galactic latitudes ($|b| < 2°$) using this combination of VVV and WISE surveys. Also, these sources presented variability in the $K_s$ light curves reported in the VIVACE catalogue (Molnar et al. 2022).

The infrared (IR) emission of AGN can be of thermal and non-thermal origin. In the case of radio-loud AGN, specifically blazar subtypes, the non-thermal character of the IR radiation is produced by the synchrotron emission of relativistic electrons within the jet. Radio continuum emission is also associated with these jets. Alternatively, in radio-quiet objects such as Seyfert galaxies, most of the radiated energy is dominated by thermal emission from the accretion disc, which is formed around the central black hole (e.g. Shakura & Sunyaev 1973). The light of the accretion disc is absorbed by the 'dust torus' (see, Netzer 2015) and re-emitted in the infrared. The emission of torus and accretion disc dominate the AGN spectral energy distribution (SED) at wavelengths longer than $\sim 1\,\mu$m up to a few tens of microns, giving the AGN distinctive red mid-IR colours (e.g. Stern et al. 2005; Richards et al. 2006; Assef et al. 2010). Therefore, IR passbands are well suited to identify AGN, as their SED are very different from those of stars and inactive galaxies. Chen, Fu & Gao (2005) studied the colour distribution of a sample of blazars and normal galaxies using the 2MASS archival data. The main results from these observations are as follows (1) the distribution of colours of blazars, in the J–H–$K_s$ colour–colour diagrams (CCD), occupy a region centered at the position (0.7; 0.7) and (2) about 30 per cent of the blazars show NIR colours indicating a possible influence from the host galaxy. Such contamination is not present at MIR wavelengths. Using WISE magnitudes, D'Abrusco et al. (2012) discovered that blazars emitting in $\gamma$-rays were clearly distinguished from other classes of galaxies and/or AGN and/or Galactic sources. *Fermi*-LAT blazars inhabit different regions in the CCD because they are dominated by non-thermal emission in the mid-IR. This two-dimensional region in the MIR CCD [3.4]–[4.6]–[12]–[22] $\mu$m was originally indicated as the WISE Gamma-ray Strip (D'Abrusco et al. 2012, WGS), and the method was improved in the WISE locus of gamma-ray blazars in D'Abrusco et al. (2013, 2014). Massaro & D'Abrusco (2016) also showed that the *Fermi*-LAT blazars are located in specific regions both in NIR and MIR CCD, clearly separated from other extragalactic sources. Stern et al. (2012) investigated the power of WISE to identify AGN based solely on the [3.4] and [4.6] magnitudes. The selection criteria of [3.4]–[4.6] $>$ 0.8 mag and [4.6] $<$ 15.05 mag produced an AGN sample with a contamination of only 5 per cent. Following this, Assef et al. (2018) presented two additional colour criteria in their AGN sample:

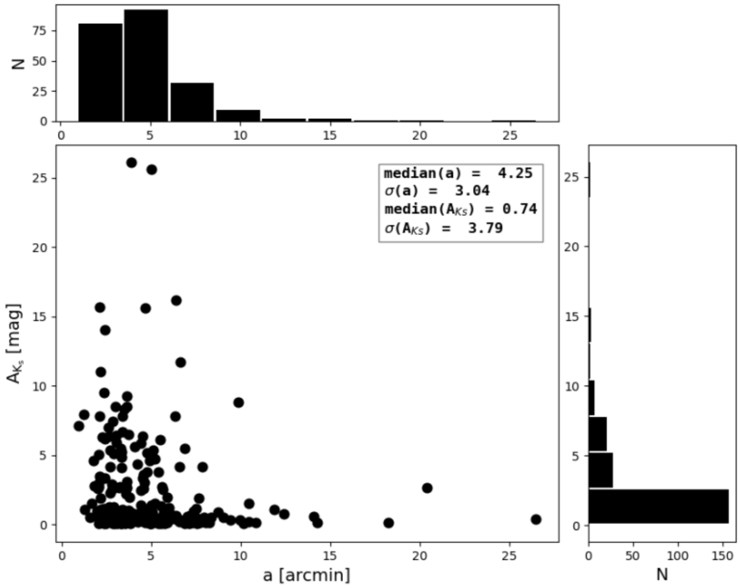


**Figure 1.** Plot resuming the interstellar extinctions in the $K_s$ passband and uncertainties in the positions of the 4FGL sources in the VVV region.



[3.4]–[4.6] > 0.5 mag and [3.4]–[4.6] > 0.77 mag, with a 90 per cent and 75 per cent completeness.

The main goal in this study is to identify, at lower Galactic latitudes, unidentified 4FGL sources with NIR and MIR counterparts using the VVV and *WISE* surveys, respectively. The paper is organised as follows. Section 2 presents the data which includes the different samples of high-energy sources together with the NIR and MIR photometry used in this study. The applied methodology to detect the counterparts is also discussed including colour–magnitude and colour-colour diagrams using VVV and WISE surveys, and the VVV $K_s$ light curves of the near-IR sources and the variability analysis. Section 3 shows the diagrams for the *Fermi*-LAT source regions with VVV candidates and the analysis of the light curves using the near-IR data. Diagrams with the WISE candidates using mid-IR data are also shown. Section 4 presents a summary of the main results.

## 2 DATA AND METHODOLOGY

### 2.1 The samples of high energy gamma-ray sources

At lower Galactic latitudes, we have found 221 4FGL sources in the bulge and disc regions covered by the VVV survey without any previous source associations at any wavelengths. Figure 1 shows the distributions of interstellar $K_s$ extinctions ($A_{Ks}$) in magnitudes and uncertainties in the positions of the *Fermi*-LAT sources as the semimajor axis (a) in arcmin of the error ellipse at 95 per cent confidence level for the 221 UGS. The median values are $A_{Ks} = 0.74 \pm 3.79$ mag and $a = 4.25 \pm 3.04$ arcmin.

According to the distributions of the interstellar extinctions and semimajor axis of the *Fermi*-LAT uncertainties, we choose to analyse sources in regions with lower interstellar extinctions ($A_{Ks} < 1.2$ mag). Taking this into account, our sample comprises 78 UGS. We defined three subsamples: the A subsample which contains 13 UGS with a < 2.5 arcmin; the B subsample that contains 12 sources with 2.5 ≤ a < 3.0 arcmin and the C subsample that contains 53 sources with 3.0 ≤ a < 5.0 arcmin. Tables 1, 2, and 3 show the positions of the UGS for the three subsamples, respectively.

Figure 2 shows the distribution in Galactic coordinates of the 78 UGS over the region covered by the VVV survey. The samples studied are highlighted as yellow squares (A subsample), green diamonds (B subsample), and orange stars (C subsample). Also the coloured UGS are over plotted on the spatial distribution of $A_V$ interstellar extinction derived from the extinction map of Schlafly & Finkbeiner (2011). The contours of the different levels correspond to 5, 10, 15, 20, 25 mag. There are 14 UGS located in the Southern disc and 64 in the bulge. The disc (bulge) UGS are 6, 3, and 5 (7, 9, and 48) in the A, B, and C subsamples, respectively.

### 2.2 Near- and mid-IR photometry

Our main goal is to identify the selected UGS with near- and mid-IR photometry counterparts using the VVV and WISE photometry, respectively. Pichel et al. (2020) analysed the four blazars located in the VVV region that were identified in the Multifrequency Catalogue of Blazars (Massaro et al. 2015) as counterparts to 3FGL sources. They defined a specific region with a radius twice the positional uncertainties associated with the high-energy sources and performed a search for all infrared sources within this area. The photometry was conducted in the five VVV passbands: Z, Y, J, H, and $K_s$ using the combination of SExtractor (Source-Extractor) + PSFEX (PSF Extractor) (Bertin 2011) to assess all the sources in the region as described in Baravalle et al. (2018). The blazars were characterised by their near- and mid-IR properties from VVV and WISE surveys, respectively showing different colours in the infrared diagrams. The photometric results of the blazar 5BZQJ1802-3940 (Pichel et al. 2020) obtained with SExtractor+PSFEX were also compared in Donoso (2020) with the data product provided by Cambridge Astronomical Survey Unit (CASU; Emerson, McPherson & Sutherland 2006). Both approaches produce comparable results and the studied blazar occupied a similar position in the CCD.

In this work, we analysed all the VVV sources with CASU photometry lying within the positional uncertainty region of the UGS. For this purpose, for each 4FGL sources, we defined a search area centred on the UGS, with radius defined by the semimajor axis of the ellipse (values reported in Table 1–3). We used the positions of the NIR sources, the object classification and the aperture magnitudes within an aperture of radius of 3 pixels, which correspond

**Table 1.** *Fermi*-LAT sources of our sample with low positional uncertainties (the A subsample). Column (1) lists the internal identification used in this work; columns (2)–(5), the 4FGL identification, the J2000 coordinates and the semimajor axis of *Fermi*-LAT error ellipse, a, at 95 per cent confidence level in arcmin taken from 4FGL, and columns (6) and (7), the VVV tile identification and the interstellar extinction in the $K_s$ passband at the source position, respectively.

| ID | 4FGL ID | RA (J2000) | Decl. (J2000) | a [arcmin] | Tile ID | $A_{Ks}$ [mag] |
|---|---|---|---|---|---|---|
| A1 | 4FGLJ1203.9-6242 | 12:03:56.23 | −62:42:34.2 | 1.272 | d040 | 1.0926 |
| A2 | 4FGLJ1317.5-6316 | 13:17:31.30 | −63:16:43.0 | 2.154 | d046 | 1.0737 |
| A3 | 4FGLJ1329.9-6108 | 13:29:56.98 | −61:08:26.2 | 1.602 | d123 | 0.5410 |
| A4 | 4FGLJ1456.7-6050 | 14:56:45.12 | −60:50:19.3 | 1.986 | d016 | 0.5663 |
| A5 | 4FGLJ1640.3-4917 | 16:40:18.63 | −49:17:19.3 | 2.304 | d029 | 0.9213 |
| A6 | 4FGLJ1712.9-4105 | 17:12:56.78 | −41:05:43.4 | 2.352 | d036 | 1.1137 |
| A7 | 4FGLJ1731.9-2719 | 17:31:55.70 | −27:19:45.8 | 2.358 | b375 | 0.5330 |
| A8 | 4FGLJ1736.1-3422 | 17:36:06.22 | −34:22:37.9 | 2.004 | b315 | 0.9297 |
| A9 | 4FGLJ1758.7-4109 | 17:58:47.20 | −41:09:10.1 | 2.082 | b215 | 0.0611 |
| A10 | 4FGLJ1759.1-3849 | 17:59:10.34 | −38:49:18.1 | 2.478 | b230 | 0.0767 |
| A11 | 4FGLJ1802.4-3041 | 18:02:27.52 | −30:41:57.1 | 2.160 | b277 | 0.2656 |
| A12 | 4FGLJ1812.8-3144 | 18:12:52.68 | −31:44:37.7 | 2.250 | b250 | 0.1417 |
| A13 | 4FGLJ1830.8-3132 | 18:30:48.79 | −31:32:11.0 | 2.394 | b209 | 0.0628 |

**Table 2.** *Fermi*-LAT sources of our sample with intermediate positional uncertainties (the B subsample). The column description is the same of Table 1.

| ID | 4FGL ID | RA (J2000) | Decl. (J2000) | a [arcmin] | Tile ID | $A_{Ks}$ [mag] |
|---|---|---|---|---|---|---|
| B1 | 4FGLJ1447.4-5757 | 14:47:25.22 | −57:57:04.0 | 2.526 | d130 | 0.6406 |
| B2 | 4FGLJ1657.7-4520 | 16:57:47.52 | −45:20:17.5 | 2.748 | d032 | 1.1385 |
| B3 | 4FGLJ1714.9-3324 | 17:14:57.14 | −33:24:48.6 | 2.946 | b370 | 0.4727 |
| B4 | 4FGLJ1721.7-3917 | 17:21:43.61 | −39:17:51.0 | 2.886 | d037 | 0.7130 |
| B5 | 4FGLJ1739.3-2531 | 17:39:20.79 | −25:31:34.3 | 2.904 | b377 | 0.6179 |
| B6 | 4FGLJ1739.7-2836 | 17:39:44.38 | −28:36:08.3 | 2.826 | b347 | 0.8319 |
| B7 | 4FGLJ1743.6-3341 | 17:43:38.55 | −33:41:38.0 | 2.694 | b302 | 0.6330 |
| B8 | 4FGLJ1748.2-1942 | 17:48:17.11 | −19:42:23.4 | 2.952 | b395 | 0.3098 |
| B9 | 4FGLJ1806.9-2824 | 18:06:58.78 | −28:24:56.9 | 2.832 | b279 | 0.2373 |
| B10 | 4FGLJ1808.4-3358 | 18:08:24.43 | −33:58:54.1 | 2.946 | b248 | 0.1017 |
| B11 | 4FGLJ1815.2-2715 | 18:15:15.15 | −27:15:26.6 | 2.952 | b267 | 0.1562 |
| B12 | 4FGLJ1817.2-3035 | 18:17:13.82 | −30:35:03.1 | 2.850 | b251 | 0.0794 |

to ∼1 arcsec (Minniti et al. 2010; Saito et al. 2010). In this way all the *Fermi*-LAT sources were surveyed in an homogeneous way.

Regarding the mid-IR, the WISE mission observed the sky in four passbands: [3.4], [4.6], [12], and [22] $\mu$m, with an angular resolution of 6.1, 6.4, 6.5, and 12.0 arcsec achieving 5$\sigma$ point-source sensitivities of 0.08, 0.11, 1, and 6 mJy, respectively, in unconfused regions on the ecliptic (Wright et al. 2010). The angular resolution in the [3.4], [4.6], and [12] $\mu$m passbands is 6 arcsec while in the [22] $\mu$m passband is 12 arcsec. All the WISE magnitudes are in the Vega system.

### 2.2.1 *Colour–Magnitude and Colour-Colour diagrams*

**Near-IR VVV survey:**

In this section, we use NIR magnitudes and colours of all the VVV objects in the regions of the 4FGL sources. The magnitudes were corrected by interstellar extinction along the line of sight, using the dust maps of Schlafly & Finkbeiner (2011) and the VVV NIR relative extinction coefficients of Catelan et al. (2011). Then, we obtained the colours for all the sources.

Baravalle et al. (2018) defined extragalactic sources using the colour criteria 0.5 < (J–$K_s$) < 2.0 mag; 0.0 < (J–H) < 1.0 mag; and 0.0 < (H–$K_s$) < 2.0 mag with the colour constraint (J–H) + 0.9 (H–$K_s$) > 0.44 mag to minimise false detections. The main result of this work is the VVV NIRGC, the catalogue of galaxies in part of the Southern Galactic disc. Massaro & D'Abrusco (2016) examined the regions in the CCD using the J, H, and $K_s$ magnitudes from the 2MASS catalogue, specifically those occupied by *Fermi*-LAT blazars. The infrared colours of the $\gamma$-ray blazars cover a distinct region, clearly separated from the other extragalactic sources. Also, Cioni et al. (2013) performed an AGN selection using the VISTA Magellanic Survey (Cioni et al. 2011, VMC). In their Figure 2, they divided the JH$K_s$ colour–colour space into four regions. AGN with a point-like morphology occupy the A region while the AGN with a detected host galaxy dominate the B region. The C region contains reddened Magellanic sources and the D region is dominated mainly by stars and low-confidence AGN. Most of the known AGN are found in the A and B regions. The appropriate cuts in colour have proven to be an extremely powerful tool for separating stellar sources from extragalactic sources. These conclusions motivate us to develop a methodology for searching for $\gamma$-ray AGN candidates within the positional uncertainty regions of the *Fermi*-LAT UGS.

Based on the results of Massaro & D'Abrusco (2016); Baravalle et al. (2023), and Cioni et al. (2011), we improved the colour cuts and we selected sources that satisfy simultaneously: 0.5 < (J–$K_s$) < 2.5 mag; 0.4 < (J–H) < 2.0 mag; 0.5 < (H–$K_s$) < 2.0 mag, and 0.2 < (Y–J) < 2.0 mag. This selection define the possible candidates

**Table 3.** *Fermi*-LAT sources of our sample with large positional uncertainties (the C subsample). The column description is the same as in Table 1.

| ID | 4FGL ID | RA (J2000) | Decl. (J2000) | a [arcmin] | Tile ID | $A_{Ks}$ [mag] |
|---|---|---|---|---|---|---|
| C1 | 4FGLJ1506.5-5708 | 15:06:32.64 | −57:08:50.6 | 3.306 | d094 | 1.0008 |
| C2 | 4FGLJ1622.0-5157 | 16:22:02.38 | −51:57:05.0 | 4.500 | d026 | 0.6612 |
| C3 | 4FGLJ1622.5-4726 | 16:22:32.38 | −47:26:05.6 | 4.992 | d142 | 0.9888 |
| C4 | 4FGLJ1628.6-4553 | 16:28:36.58 | −45:53:47.4 | 4.290 | d144 | 0.5998 |
| C5 | 4FGLJ1717.5-4022 | 17:17:34.63 | −40:22:43.7 | 3.720 | d037 | 0.7776 |
| C6 | 4FGLJ1722.1-3205 | 17:22:06.67 | −32:05:16.4 | 3.330 | b358 | 0.6575 |
| C7 | 4FGLJ1726.8-2659 | 17:26:50.79 | −26:59:56.4 | 4.140 | b389 | 0.4855 |
| C8 | 4FGLJ1730.3-2913 | 17:30:18.44 | −29:13:48.7 | 4.692 | b360 | 0.5339 |
| C9 | 4FGLJ1730.8-3806 | 17:30:53.28 | −38:06:47.2 | 3.960 | b299 | 0.8399 |
| C10 | 4FGLJ1732.0-2659 | 17:32:00.02 | −26:59:20.4 | 4.398 | b375 | 0.6279 |
| C11 | 4FGLJ1733.2-2915 | 17:33:13.70 | −29:15:25.6 | 3.696 | b360 | 0.5950 |
| C12 | 4FGLJ1734.0-2933 | 17:34:03.07 | −29:33:02.9 | 3.156 | b360 | 0.6732 |
| C13 | 4FGLJ1734.5-2818 | 17:34:35.52 | −28:18:07.9 | 3.948 | b361 | 0.5351 |
| C14 | 4FGLJ1737.2-2421 | 17:37:13.92 | −24:21:58.7 | 3.324 | b391 | 0.4342 |
| C15 | 4FGLJ1737.3-3332 | 17:37:22.35 | −33:32:01.3 | 3.756 | b316 | 0.9934 |
| C16 | 4FGLJ1738.1-2453 | 17:38:10.20 | −24:53:37.3 | 4.650 | b377 | 0.4810 |
| C17 | 4FGLJ1738.8-3418 | 17:38:53.40 | −34:18:36.0 | 4.920 | b302 | 0.8755 |
| C18 | 4FGLJ1739.2-2717 | 17:39:16.35 | −27:17:42.4 | 4.416 | b362 | 0.4516 |
| C19 | 4FGLJ1740.7-2640 | 17:40:44.57 | −26:40:37.2 | 3.426 | b362 | 0.7807 |
| C20 | 4FGLJ1741.1-3328 | 17:41:10.39 | −33:28:04.4 | 4.908 | b302 | 0.7213 |
| C21 | 4FGLJ1741.3-3357 | 17:41:22.80 | −33:57:23.4 | 4.446 | b302 | 0.5486 |
| C22 | 4FGLJ1742.8-2246 | 17:42:53.88 | −22:46:18.5 | 4.542 | b379 | 0.2885 |
| C23 | 4FGLJ1743.4-2406 | 17:43:28.23 | −24:06:14.4 | 4.116 | b378 | 0.2891 |
| C24 | 4FGLJ1744.9-3322 | 17:44:56.07 | −33:22:19.9 | 4.494 | b303 | 0.6032 |
| C25 | 4FGLJ1745.6-3626 | 17:45:39.34 | −36:26:17.9 | 3.744 | b273 | 0.3488 |
| C26 | 4FGLJ1746.1-2541 | 17:46:11.54 | −25:41:17.2 | 3.240 | b349 | 0.5557 |
| C27 | 4FGLJ1747.0-3505 | 17:47:05.02 | −35:05:56.0 | 3.072 | b288 | 0.2421 |
| C28 | 4FGLJ1747.7-2141 | 17:47:45.58 | −21:41:22.9 | 4.374 | b380 | 0.4450 |
| C29 | 4FGLJ1747.9-3224 | 17:47:56.28 | −32:24:45.4 | 3.390 | b303 | 1.0774 |
| C30 | 4FGLJ1750.6-1906 | 17:50:39.46 | −19:06:36.4 | 3.402 | b396 | 0.3183 |
| C31 | 4FGLJ1750.9-3301 | 17:50:55.15 | −33:01:12.4 | 3.918 | b289 | 0.3749 |
| C32 | 4FGLJ1752.3-2914 | 17:52:18.53 | −29:14:57.1 | 3.330 | b320 | 0.3951 |
| C33 | 4FGLJ1752.3-3139 | 17:52:20.26 | −31:39:07.6 | 3.390 | b290 | 0.5927 |
| C34 | 4FGLJ1753.3-3325 | 17:53:23.93 | −33:25:00.8 | 4.224 | b275 | 0.2869 |
| C35 | 4FGLJ1754.6-2933 | 17:54:39.14 | −29:33:06.5 | 3.456 | b306 | 0.2992 |
| C36 | 4FGLJ1754.8-3200 | 17:54:48.79 | −32:00:02.5 | 3.978 | b290 | 0.3613 |
| C37 | 4FGLJ1757.4-3125 | 17:57:24.94 | −31:25:07.3 | 3.792 | b291 | 0.3970 |
| C38 | 4FGLJ1758.0-2953 | 17:58:02.52 | −29:53:21.5 | 3.786 | b292 | 0.3889 |
| C39 | 4FGLJ1758.3-1920 | 17:58:23.09 | −19:20:36.2 | 4.224 | b368 | 0.7412 |
| C40 | 4FGLJ1800.5-2910 | 18:00:30.10 | −29:10:24.6 | 4.200 | b292 | 0.2789 |
| C41 | 4FGLJ1801.0-2802 | 18:01:02.90 | −28:02:21.5 | 4.002 | b307 | 0.3531 |
| C42 | 4FGLJ1802.1-2652 | 18:02:10.51 | −26:52:17.0 | 4.518 | b308 | 0.8211 |
| C43 | 4FGLJ1805.1-3618 | 18:05:06.36 | −36:18:21.6 | 3.114 | b232 | 0.0789 |
| C44 | 4FGLJ1808.4-3522 | 18:08:28.51 | −35:22:24.6 | 3.330 | b233 | 0.0759 |
| C45 | 4FGLJ1808.5-3701 | 18:08:30.43 | −37:01:50.2 | 3.288 | b218 | 0.0520 |
| C46 | 4FGLJ1809.2-2726 | 18:09:13.82 | −27:26:44.2 | 4.218 | b280 | 0.1862 |
| C47 | 4FGLJ1811.0-2725 | 18:11:03.44 | −27:25:19.2 | 4.302 | b280 | 0.1787 |
| C48 | 4FGLJ1814.7-3420 | 18:14:45.75 | −34:20:28.3 | 3.564 | b234 | 0.0652 |
| C49 | 4FGLJ1816.4-2727 | 18:16:25.47 | −27:27:22.7 | 4.698 | b266 | 0.1222 |
| C50 | 4FGLJ1817.9-3334 | 18:17:55.17 | −33:34:21.7 | 3.846 | b221 | 0.0635 |
| C51 | 4FGLJ1819.9-2926 | 18:19:57.58 | −29:26:20.8 | 4.992 | b252 | 0.0920 |
| C52 | 4FGLJ1820.7-3217 | 18:20:45.81 | −32:17:26.5 | 4.944 | b222 | 0.0726 |
| C53 | 4FGLJ1828.2-3252 | 18:28:13.49 | −32:52:10.6 | 4.998 | b208 | 0.0599 |

to be related to UGS. In addition to the colour selection, a visual inspection of the candidates in the five passbands of the survey was performed. In case of doubts, we created the false-colour red-green-blue (RGB) images using the $K_s$, H, and J passbands. Figure 3 shows some examples of these sources as $1' \times 1'$ VVV colour composed images. We eliminated objects with strong contamination by bright nearby stars and those sources that have fainter $K_s$ magnitudes.

**Mid-IR: WISE**

We applied the methodology used in Pichel et al. (2020) and D'Abrusco et al. (2019) to all the *Fermi*-LAT sources. For the analysis, unless stated otherwise, we considered only WISE sources detected with a minimum signal-to-noise ratio of 7 in at least one passband. Using the WGS and the WISE locus method described in D'Abrusco et al. (2019), we applied the criterion that blazars lie in

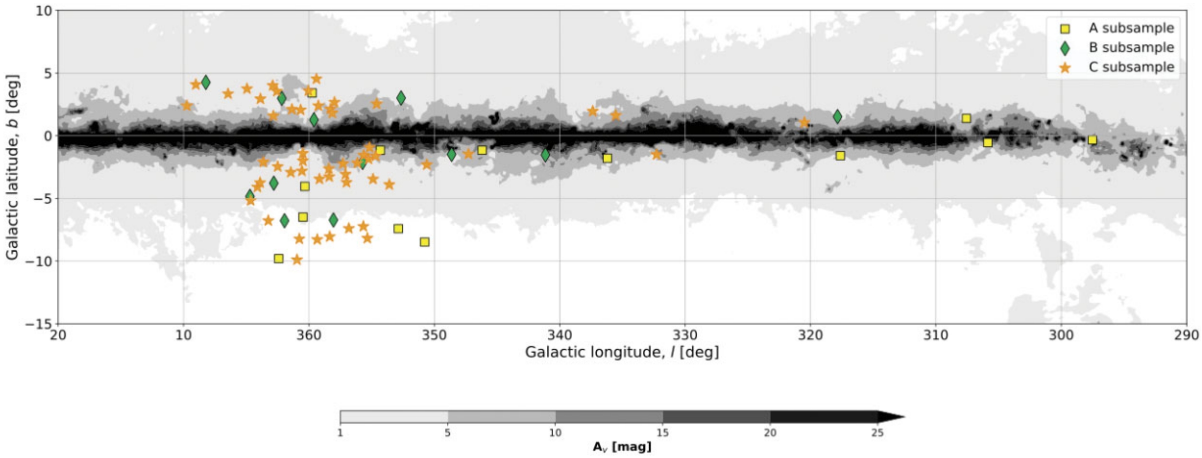


**Figure 2.** The distribution of the 78 UGS in the VVV region using different symbols for A, B, and C subsamples. The $A_V$ iso-contours at 5, 10, 15, 20, 25 mag derived from the extinction maps of Schlafly & Finkbeiner (2011) are superposed.

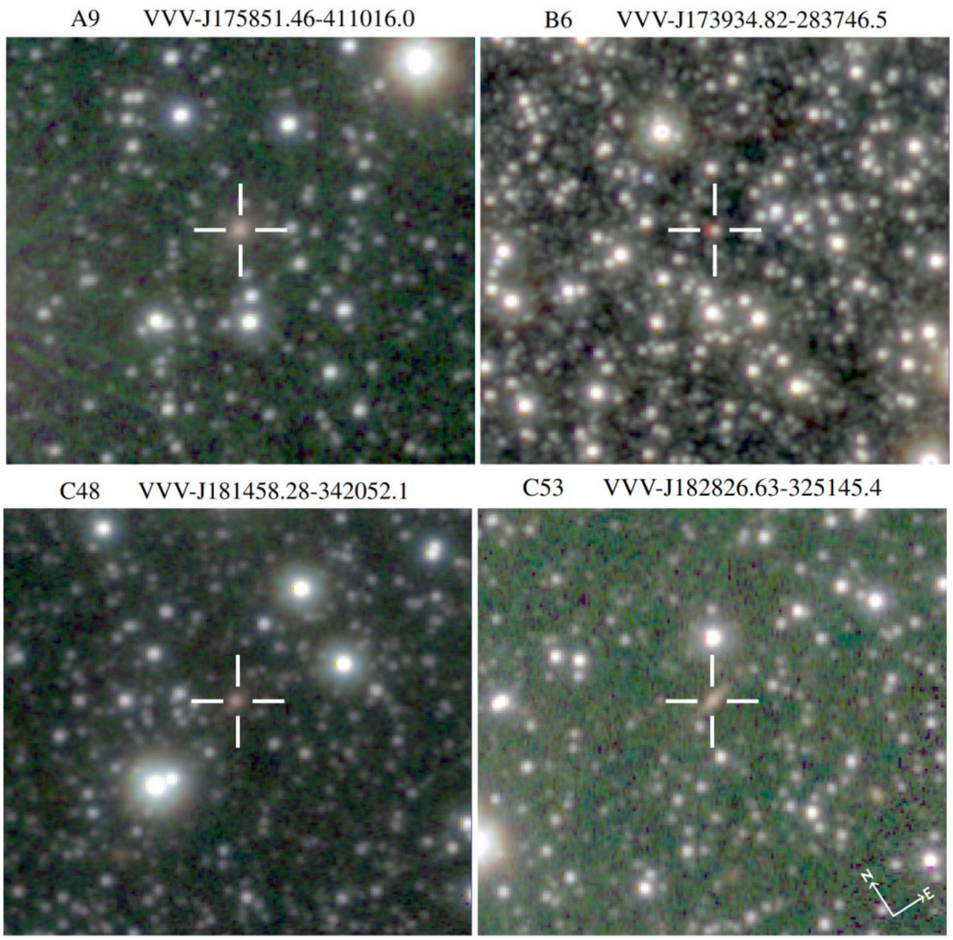


**Figure 3.** $1' \times 1'$ VVV colour composed images of some cases belonging to our sample of sources. The orientation is shown in the bottom-right panel.

a distinctive region in the 3D MIR CCD using photometry at [3.4], [4.6], [12], and [22] $\mu$m. The identification of WISE blazar candidates involved a selection process based on 2D projections within the CCD using the WISE locus method, as described previously. This technique may offer multiple possibilities depending on the number of identified candidates. When there is just one candidate, it is assumed to be directly associated with the *Fermi*-LAT source. Nevertheless, in cases with more candidates it is difficult to determine which one is associated, making further studies essential. In addition, to improve our selection of WISE candidates, we included AGN candidates using the criteria outlined in studies by Stern et al. (2012) and Assef et al. (2018). All identified WISE blazar candidates are also considered to be WISE AGN candidates, so all WISE candidates.

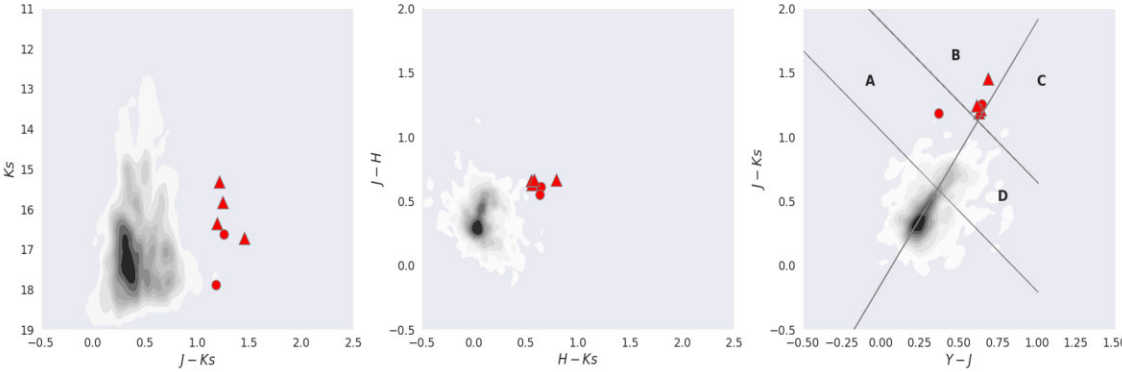


**Figure 4.** CMD and CCD for the field of *Fermi*-LAT source A9. Left, central, and right panels report (J–$K_s$)-$K_s$ CMD, (H–$K_s$)-(J–H), and (Y–J)-(J–$K_s$) CCD using near-IR data from the VVV survey, respectively. The targets in red are those showing extended morphology in the images. The objects marked with circles do not have reliable variability curves; thus, the variability analysis was not performed on these targets. The objects indicated by filled triangles are those for which the variability analysis demonstrates their nature as variable sources. Grey lines defined by Cioni et al. (2013) are drawn on the YJ$K_s$ CCD and labels of regions defined by those authors are also indicated. Grey-scale contours correspond to density of the NIR objects, lying within the positional uncertainty region of the UGS.

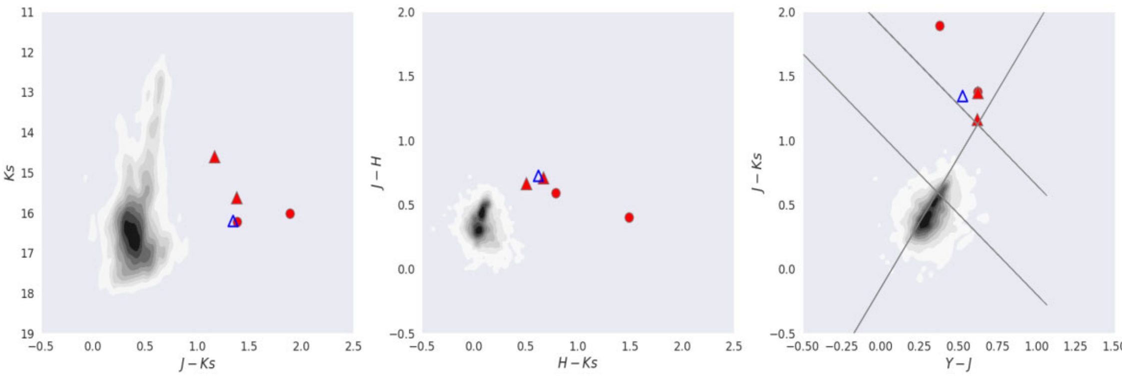


**Figure 5.** As Fig. 4, but for *Fermi* source A12. Empty blue triangle represents an object with low or negligible variability and the blue colour indicates a point-like appearance.

### 2.2.2 *Variability analysis with the VVV photometry*

Here, we performed the variability analysis for the objects associated to the *Fermi*-LAT sources. We have obtained the $K_s$ passband light curves using the second version of VVV Infrared Astrometric Catalogue (VIRAC2; see Smith et al. 2018 and Smith et al. in preparation). This is photometry based on PSF. We selected the measurements with photometric flags equal to 0 (see the catalogue) in order to obtain reliable light curves. Their coordinates were cross-matched with the VIRAC2 assuming differences in their positions of 1 arcsec. Twenty seven good light curves have a five astrometric parameter solution (a de-facto 10 epoch selection), not flagged as a probable duplicate, detected in more than 20 per cent of the observations that cover the source, and with a unit weight error less than 1.8. On the contrary, the rejected objects have not met the above criteria because they are highly contaminated with nearby stars or they are too faint to have reliable magnitudes.

In order to investigate the variability of these objects, we applied the methodology used in Pichel et al. (2020). We examined the fractional variability amplitude, $\sigma_{\rm rms}$ (Nandra et al. 1997; Edelson et al. 2002; Sandrinelli et al. 2014; Pichel et al. 2020) defined as $\sigma^2_{rms} = \frac{1}{N\mu^2}\sum_{i=1}^{N}[(F_i-\mu)^2-\epsilon_i^2]$, where N represents the number of flux values $F_i$ with their uncertainties $\epsilon_i$, and $\mu$ denotes the average flux. This parameter represents the excess variability that cannot be solely attributed to flux errors. Also, we investigated the slope of the light curves, taking into consideration the results of Cioni et al. (2013) that more than 75 per cent of QSO in the VCM survey exhibit a slope variation in the $K_s$ passband larger than $10^{-4}$ mag/day. They defined the slope of the overall $K_s$ variation in the light curves that were sampled over a range of 300-600 days, 40-80 days, or shorter. In this analysis we followed the same procedure as Baravalle et al. (2023), we performed a linear fit of the $K_s$ light curves, considering a range of days defined by the highest and lowest variations observed in the light curve. In all light curves, the range of days considered for this analysis varies from 1200 to ∼2300 days (Baravalle et al. 2023).

## 3 RESULTS

On the basis of the methodology detailed earlier, here, the VVV ZYJH$K_s$ magnitudes, colours, and $K_s$ light curves of the AGN candidates are presented. As explained in subsection 2.2.1, we have constructed colour–magnitude and colour-colour diagrams for each 4FGL. For those 4FGL sources with candidate counterparts, the (J–$K_s$)-$K_s$, colour–magnitude diagram (CMD), and (H–$K_s$)-(J–H) and (Y–J)-(J–$K_s$) CCD are shown in the Figures 4–17. There, grey-scale contours correspond to density of all the CASU objects found in 4FGL regions with size defined by the positional uncertainty of the *Fermi*-LAT source, including stellar and extragalactic sources. The regions preferentially populated for AGN candidates are 0.5 < (J–$K_s$) < 2.5 mag; 0.5 < (H–$K_s$) < 2.0 mag; 0.4 < (J–H) < 2.0 mag;

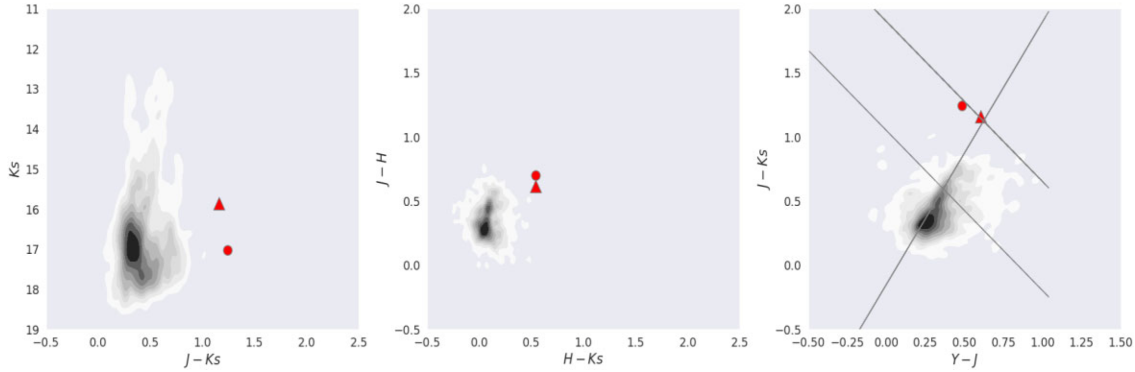

**Figure 6.** As Fig. 4, but for *Fermi* source A13.

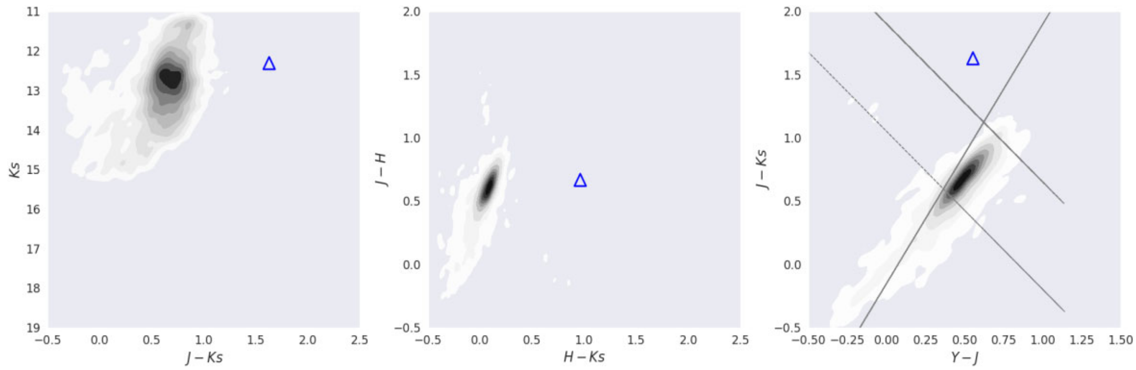

**Figure 7.** As Fig. 4, but for *Fermi* source B6. Empty blue triangle represents the candidate with low or negligible variability and the blue colour indicates a point-like morphology.

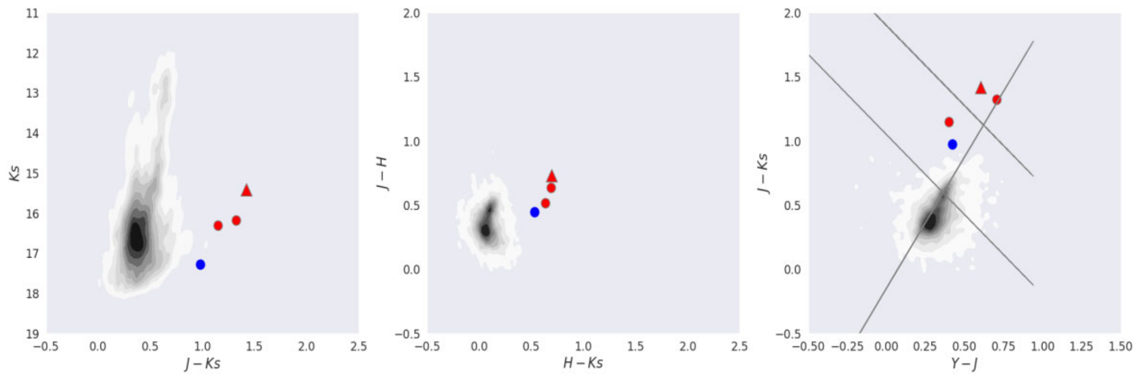

**Figure 8.** As Fig. 4, but for *Fermi* source B12. The candidate with point-like morphology is indicated by blue circle.

and 0.2 < (Y–J) < 2.0 mag. The candidates were highlighted and represented by red circles for extended sources and as blue circles for objects with point-like morphology. Those AGN candidates that present variability are indicated by triangles, the colour depending on the origin of the sources: red for galaxy-like sources and blue for stellar-like objects. Full triangles are objects that have slope in $K_s$ passband higher than $10^{-4}$ mag/day and empty triangles have slopes lower than this value. Also, the regions limited with lines as defined by Cioni et al. (2013) are shown.

After careful visual inspection, we eliminated faint and contaminated sources, leaving only those that were considered VVV candidates. Thus, 7 *Fermi*-LAT sources have only one VVV candidate: A13, B6, B12, C40, C46, C47, and C51. Some UGS have more than one VVV candidate: the *Fermi*-LAT source C53 presents 5 candidates; A9, 4 candidates; A12, 3 candidates; and C44, C48, C50 and C52, 2 candidates each one. These VVV candidates are not located in the Southern disc and therefore, there are no sources in common with the VVV NIRGC.

In Figure 18, we present the differential $K_s$ light curves of the VVV sources. These curves represent the $K_s$ magnitudes with the median subtracted, sampled over a period covering more than 2500 days. We noted that the overall shape of light curves is irregular, lacking any discernible periodic pattern. In some cases, we observe prominent fluctuations in brightness that resemble peaks, exhibiting statistical significance well above the value of the associated uncertainties. Table 4 presents the main results of the $K_s$ variability of these sources,

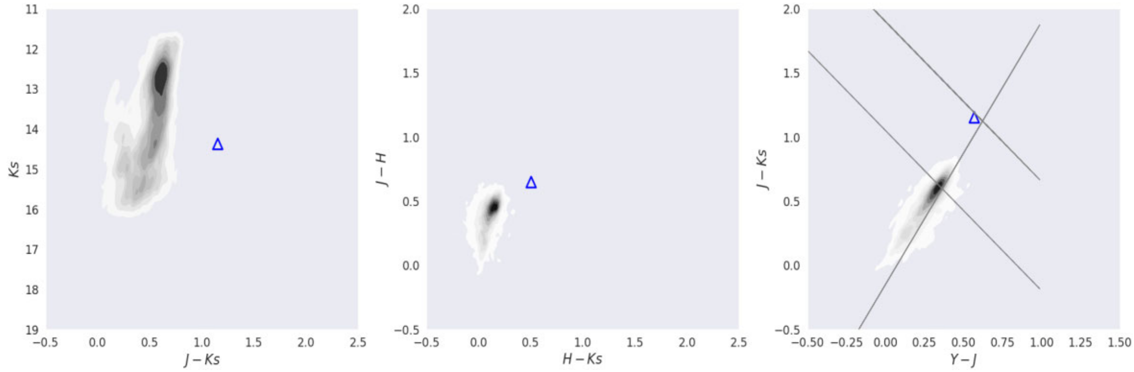


**Figure 9.** As Fig. 4, but for *Fermi* source C40. Empty blue triangle represents an object with low or negligible variability and the blue colour indicates a point-like appearance.

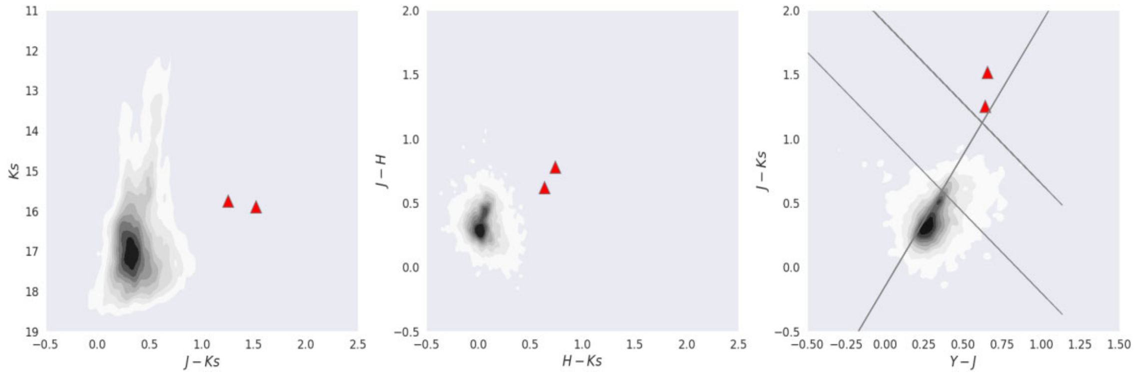


**Figure 10.** As Fig. 4, but for *Fermi* source C44.

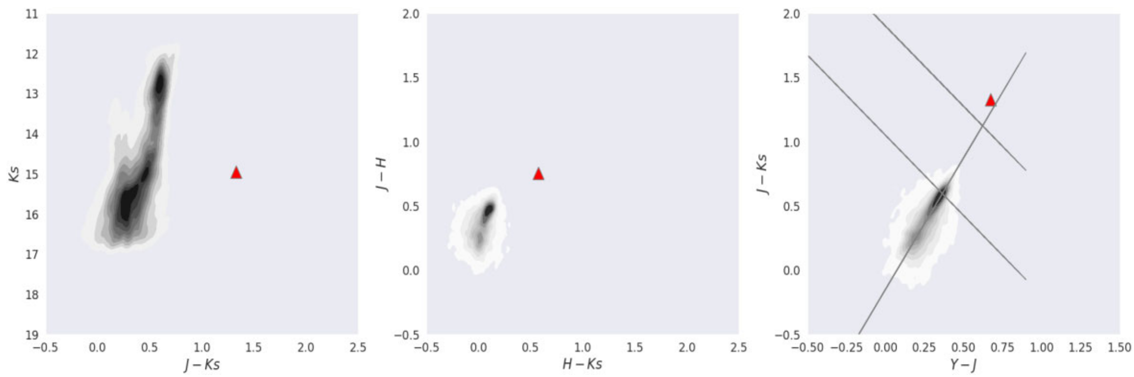


**Figure 11.** As Fig. 4, but for *Fermi* source C46.

showing the mean magnitude, $\sigma_{\rm rms}$ and the slope of the linear fits with the range of days used. Also some comments of the visual inspection of the objects are included. Most of them are early type galaxies or the bulges of galaxies, because the NIR is sensitive to detecting the oldest stellar population in the galaxy. We did not include in the analysis those objects with strong crowding contamination or faint magnitudes as mentioned above. In general, most of the studied objects exhibit moderate variability, characterised by $\sigma_{\rm rms}$ values ranging from 12.5 to 32.1. These results are in agreement with previous studies on type-1 AGN, such as those by Nandra et al. (1997); Edelson et al. (2002); Baravalle et al. (2023). However, these values are lower than those reported for blazars (e.g. Sandrinelli et al. 2014; Pichel et al. 2020). Since type-1 AGN typically present lower variability amplitudes than blazars (e.g. Ulrich et al. 1997; Mao & Yi 2021), our results suggest that these objects are potential type-1 AGN, such as quasars or Seyfert 1 galaxies. Moreover, the observed light-curve slopes are $\geq 10^{-4}$ mag/day, comfortably lying within the limit established by Cioni et al. (2013) for quasars. Alternatively, there are four objects that present negligible variability, with very low values of $\sigma_{\rm rms}$. These objects are VVV-J181300.69-314505.6, VVV-J173934.82-283746.5, VVV-J180027.63-291007.4, and VVV-J181803.69-333215.7 in the regions of the *Fermi*-LAT sources A12, B6, C40, and C50, respectively (see Figure 18 and Table 4). As expected, these objects also exhibit significantly lower slope values, typically below $10^{-5}$ mag/day. Although luminosity variability is a common feature of AGN, the absence of variability does not

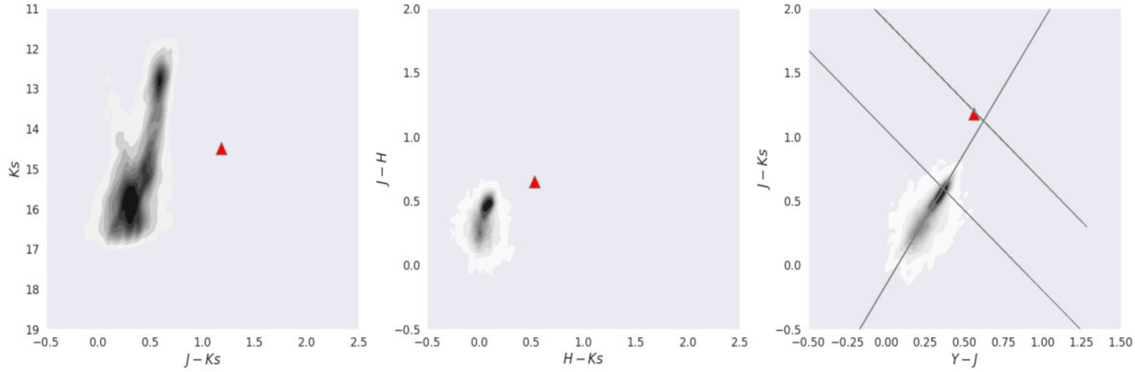


**Figure 12.** As Fig. 4, but for *Fermi* source C47.

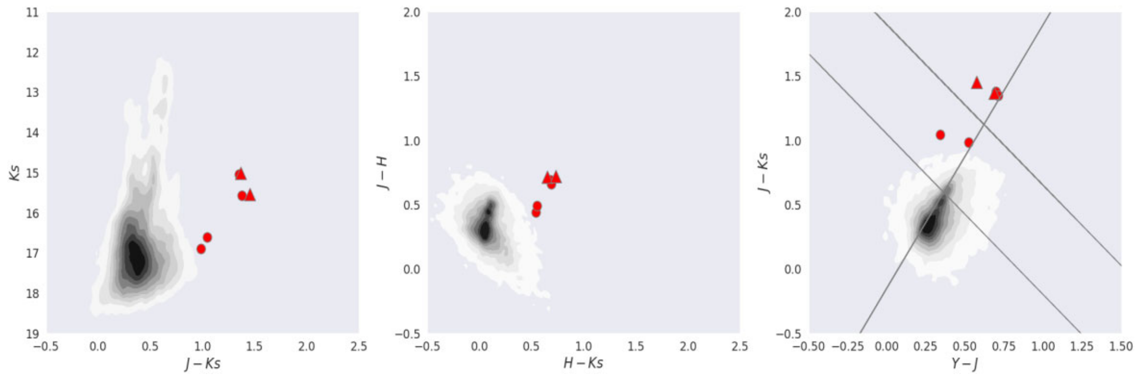


**Figure 13.** As Fig. 4, but for *Fermi* source C48.

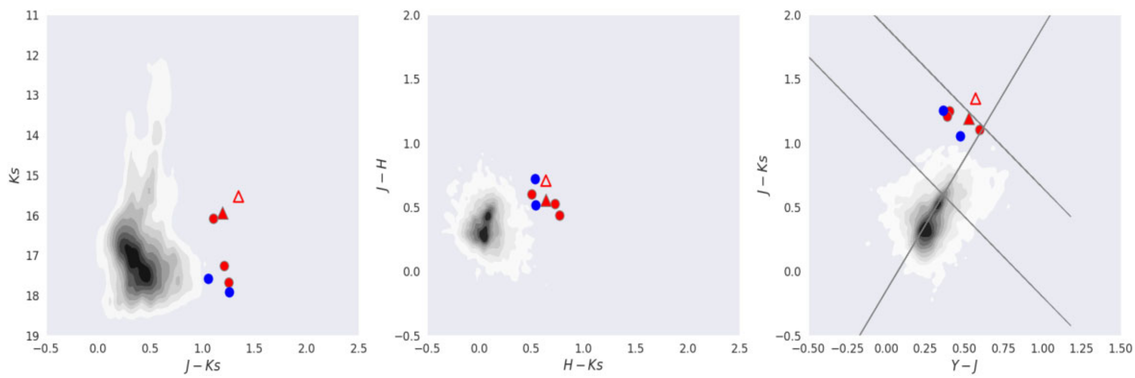


**Figure 14.** As Fig. 4, but for *Fermi* source C50. Empty red triangle represents an object with low or negligible variability and the red colour indicates a extended appearance.

necessarily rule out the possibility of an object being an AGN. It is important to note that not all AGN exhibit the same degree of variability, and certain AGN may display very low or nearly negligible levels of variability (e.g. Ilić et al. 2017; Li et al. 2022; Pennock et al. 2022). Beyond this, more than 85 per cent of the objects studied here show a moderate variability, and as mentioned above, these results suggest that these sources are type-1 AGN candidates. It has to be noted that this analysis is based only with photometric data. A spectroscopic study is necessary in order to investigate the nature and type of AGN.

We also searched for WISE candidates coincident with the position of the VVV candidates found before. We could not get any match between the VVV and WISE candidates with the exception of the source VVV-J173934.82-283746.5 in the *Fermi*-LAT B6 region. This object has a source at an angular distance of 0.64 arcsec classified as the OH/IR star 359.54+01.29 (Sevenster et al. 1997).

The WISE results are not as clear as those in Pichel et al. (2020) and Baravalle et al. (2023). All 4 sources explored in Pichel et al. (2020) had VVV candidate counterparts, but only two of them had WISE ones. In Baravalle et al. (2023), the 4 active galaxies had VVV and WISE counterparts. The main difference between these two studies and the present one is that the VVV candidates were brighter in the $K_s$ passband. Here, all the VVV candidates are in the range of 14.5 to 18 mag with the exception of the candidate in the *Fermi*-LAT B12 region. Another difference is the high interstellar extinction towards the fields studied here and in some cases, strong stellar contamination.

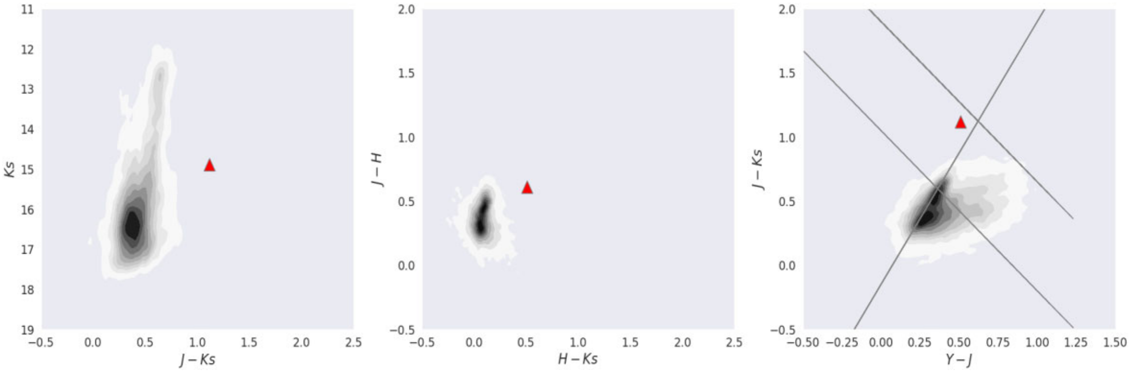


**Figure 15.** As Fig. 4, but for *Fermi* source C51.

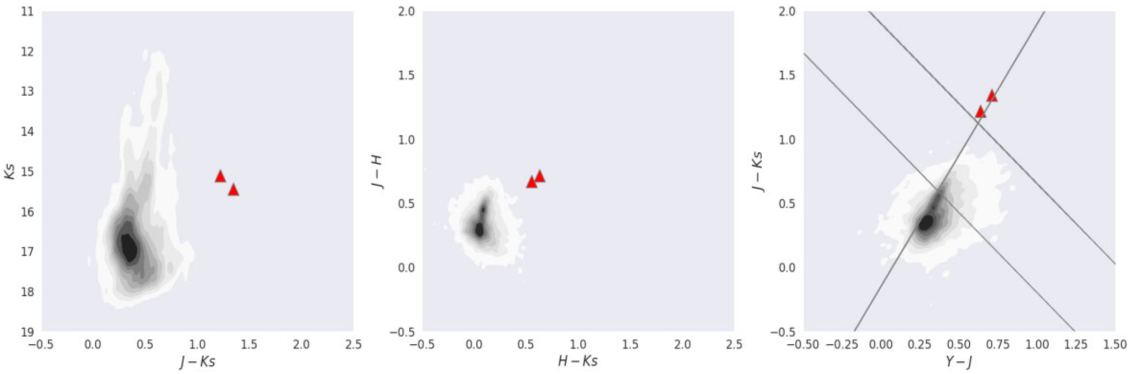


**Figure 16.** As Fig. 4, but for *Fermi* source C52.

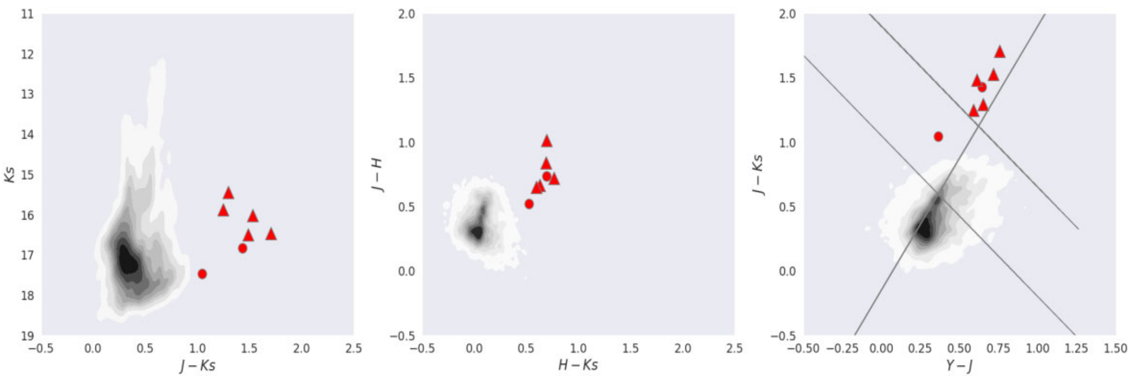


**Figure 17.** As Fig. 4, but for *Fermi* source C53.

In the mid-IR, the results here are more noisy in general. Based on these results, we present candidates in the *Fermi*-LAT source regions both in the NIR and MIR using VVV and WISE surveys, respectively. However, inside the *Fermi*-LAT source A8 appears a WISE source (J173612.07-342204.7) that satisfies all the criteria to be a blazar candidate using the WGS method. This region has a high interstellar extinction ($A_{Ks} = 0.9297$ mag) and the NIR CMD shows bright magnitudes without candidates to counterparts. Also, for the *Fermi*-LAT source B10, two WISE AGN/blazar candidates were found (J180835.96-335752.2 and J180825.25-335615.1) using the WGS and Assef et al. (2018) methods for AGN. In Figure 19 both *Fermi*-LAT sources are shown, using the mid-IR [3.4]–[4.6] versus [4.6]–[12], [3.4]–[4.6] versus [12]–[22], and [4.6]–[12] versus [12]–[22] CCD of all the WISE sources (represented with black dots). The red box indicates the limits used to identify QSO and Seyfert galaxies (Jarrett et al. 2011). These WISE candidates do not have VVV counterparts; thus, no other analysis and cross-match can be done in this paper. Further analysis with IR spectroscopy is needed in order to establish the nature of the WISE sources.

We might note that most of the VVV candidates are found in the B region of the CCD defined by Cioni et al. (2013). Our sample of VVV candidates are centered at the position (0.6; 0.7) in the CCD (J–H) versus (H–$K_s$) according to Chen, Fu & Gao (2005). For the 27 candidates listed in Table 4, we then searched for the closest object

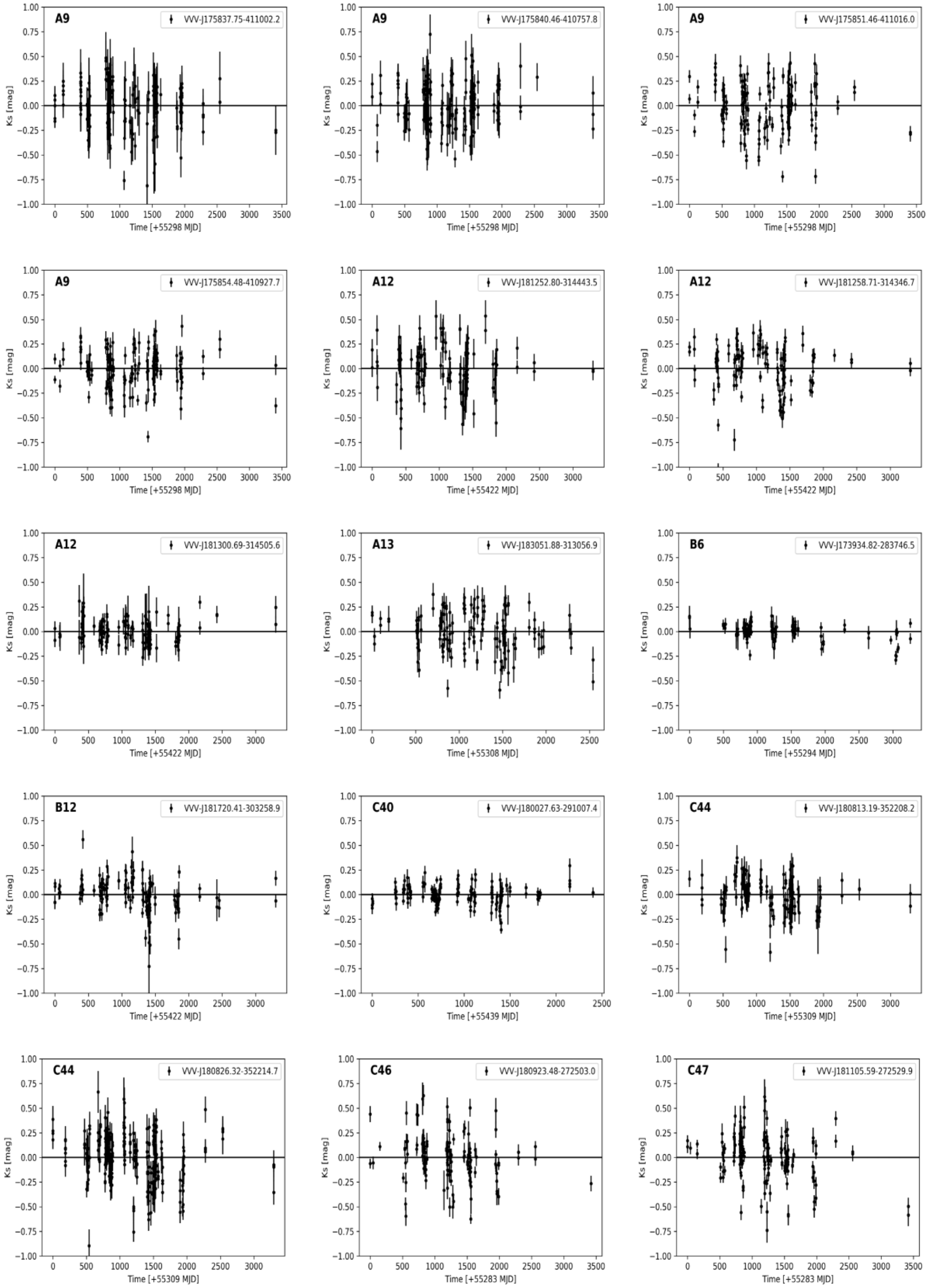


**Figure 18.** $K_s$ differential light curves of the VVV sources for the A, B, and C subsamples.

in a circle of 30 arcsec radius using the SIMBAD data base[1] and we have not found any catalogued source, with the exception of the object in the region of the *Fermi*-Lat source B6 mentioned above. There have been no previous photometry or spectroscopy studies performed in these regions.

[1] https://cds.unistra.fr/

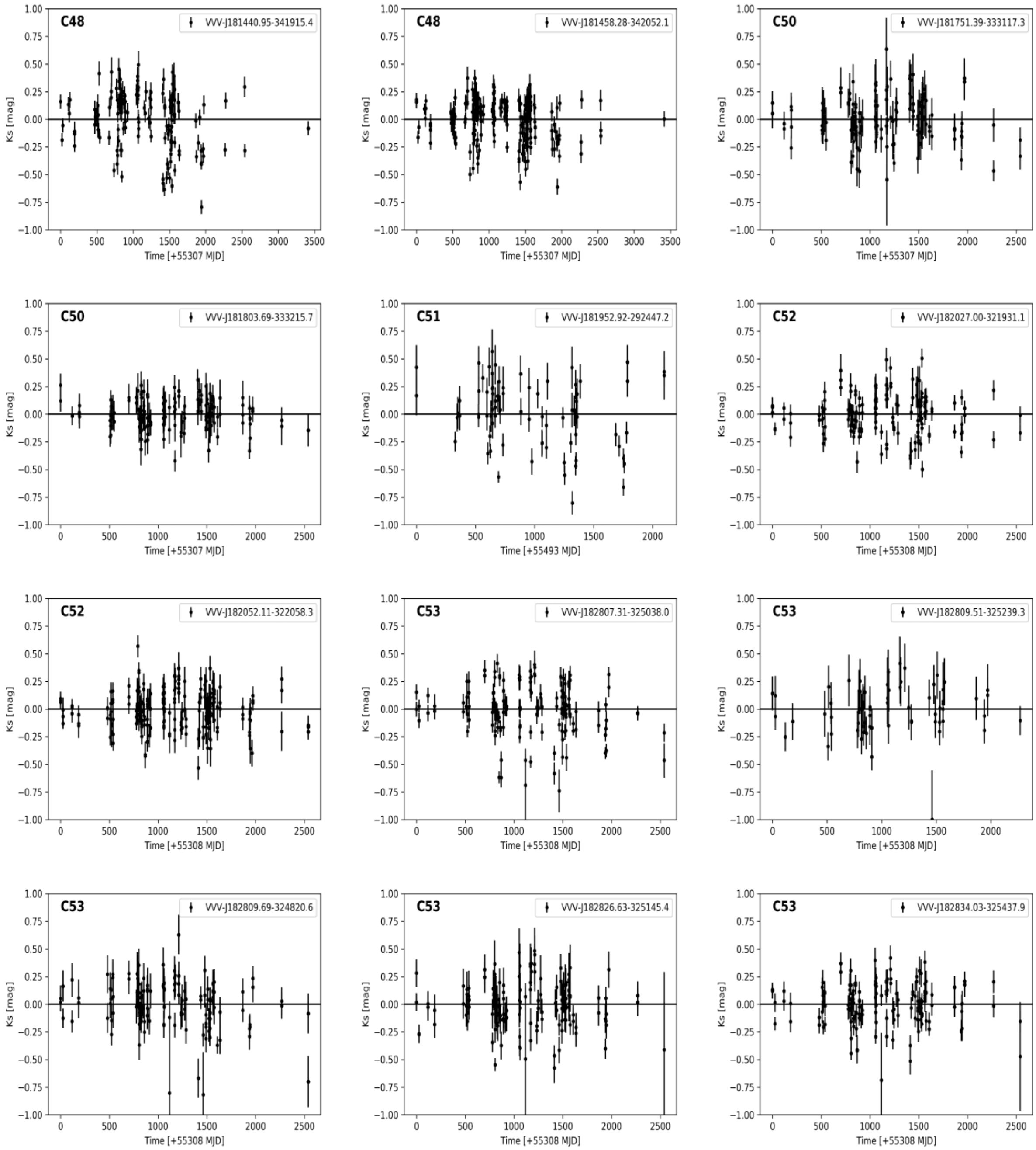


**Figure 18.** continued

Lefaucheur & Pita (2017) obtained a sample of 595 blazar candidates from the unassociated sources within the 3FGL catalogue (Acero & Ackermann 2015). They proceeded to train multivariate classifiers on samples derived from the *Fermi*-LAT catalogue, carefully selecting discriminant parameters. Within their blazar candidates, there are 30 objects in the region of the VVV survey, of which A5, B3, B4, C10, C27, and C49 in our subsamples. They classified the *Fermi*-LAT source A5 as BL Lac, however, there are no VVV candidates in this region because of the high interstellar extinction ($A_{Ks} = 0.9213$ mag). The *Fermi*-LAT C10 was also classified as BL Lac and the near-IR CMD and CCD show that there are a point-like and a galaxy-like objects in the region that we have defined as possible VVV candidates. This is a region of strong crowding contamination and the $K_s$ light curves of these two objects were noisy and did not satisfy our criteria. For these reasons there are no other VVV nor WISE candidates in common with these authors.

All the *Fermi*-LAT sources in the A subsample with AGN candidates are found in regions with smaller interstellar extinctions ($A_{Ks} < 0.15$ mag). In the B subsample, there are only two *Fermi*-LAT sources associated with VVV AGN candidates: B12 has interstellar extinction lower than 0.10 mag and B6 is in a region with high interstellar extinction. Hence, an interesting feature of B6 source's colour–magnitude diagram is that the $K_s$ magnitudes are brightest compared to the other diagrams (Figure 7). In the C subsample most of the cases have $A_{Ks} < 0.10$ mag with the exception of C40, C46, and C47 with values from 0.17 to 0.28 mag approximately. For the other

**Table 4.** $K_s$ variability of the near-IR sources from the VVV survey. The internal identification of the 4FGL sources in the subsamples is listed in column (1); the VVV and the VIRAC2 identifications of the sources is in columns (2) and (3), respectively; the mean $K_s$ magnitude from VIRAC2 is in column (4); the fractional variability amplitude is in column (5); the range of days considered to derive the slope is in column (6); the absolute value of the slope of the variation is in column (7); and comments after the visual inspection of the sources is in column (8).

| ID | VVV ID | VIRAC2 ID | $K_s$ [mag] | $\sigma_{rms}$ ($\times$ 100 per cent) | Range of days [mag/day] | Slope variation | Visual classification |
|---|---|---|---|---|---|---|---|
| A9 | VVV-J175837.75-411002.2 | 14 627 836 000 675 | 17.02 ± 0.23 | 16.3 | 600–1800 | 0.00013 | Early-type galaxy |
| A9 | VVV-J175840.46-410757.8 | 14 623 740 001 044 | 17.70 ± 0.21 | 16.0 | 1000–2700 | 0.00016 | Early-type galaxy |
| A9 | VVV-J175851.46-411016.0 | 14 627 837 002 111 | 15.89 ± 0.24 | 22.5 | 0–1400 | 0.00016 | Early-type galaxy |
| A9 | VVV-J175854.48-410927.7 | 14 627 837 000 010 | 16.20 ± 0.18 | 16.2 | 300–1400 | 0.00013 | Early-type galaxy |
| A12 | VVV-J181252.80-314443.5 | 13 796 388 005 480 | 16.24 ± 0.23 | 19.2 | 0–1300 | 0.00015 | Early-type galaxy |
| A12 | VVV-J181258.71-314346.7 | 13 792 293 006 414 | 15.30 ± 0.26 | 31.6 | 0–1300 | 0.00020 | Early-type galaxy |
| A12 | VVV-J181300.69-314505.6 | 13 800 485 003 177 | 16.22 ± 0.11 | 3.3 | 300–1600 | 0.00008 | Faint galaxy |
| A13 | VVV-J183051.88-313056.9 | 13 775 960 000 711 | 16.36 ± 0.20 | 17.2 | 1000–2600 | 0.00017 | Early-type galaxy |
| B6 | VVV-J173934.82-283746.5 | 13 501 381 012 265 | 13.91 ± 0.08 | 5.0 | 0–3200 | 0.00005 | Point-like morphology |
| B12 | VVV-J181720.41-303258.9 | 13 685 809 002 107 | 15.86 ± 0.16 | 14.0 | 250–1700 | 0.00015 | Early-type galaxy |
| C40 | VVV-J180027.63-291007.4 | 13 554 689 002 540 | 14.91 ± 0.10 | 6.8 | 250–2000 | 0.00004 | Faint galaxy |
| C44 | VVV-J180813.19-352208.2 | 14 128 151 000 796 | 16.28 ± 0.16 | 12.5 | 700–3300 | 0.00010 | Early-type galaxy |
| C44 | VVV-J180826.32-352214.7 | 14 128 152 000 807 | 16.49 ± 0.23 | 20.8 | 0–3300 | 0.00010 | Early-type galaxy |
| C46 | VVV-J180923.48-272503.0 | 13 382 683 008 897 | 15.58 ± 0.23 | 20.3 | 700–3420 | 0.00013 | Faint galaxy |
| C47 | VVV-J181105.59-272529.9 | 13 386 783 001 943 | 15.30 ± 0.23 | 22.1 | 0–3420 | 0.00012 | Early-type galaxy |
| C48 | VVV-J181440.95-341915.4 | 14 033 961 000 873 | 15.81 ± 0.26 | 24.8 | 700–3420 | 0.00017 | Early-type galaxy |
| C48 | VVV-J181458.28-342052.1 | 14 033 962 001 744 | 16.03 ± 0.18 | 16.1 | 700–2550 | 0.00012 | Early-type galaxy |
| C50 | VVV-J181751.39-333117.3 | 13 960 242 002 550 | 16.55 ± 0.19 | 13.6 | 1000–2550 | 0.00016 | Late-type galaxy |
| C50 | VVV-J181803.69-333215.7 | 13 960 243 002 545 | 16.56 ± 0.13 | 8.0 | 0–2550 | 0.00002 | Early-type galaxy |
| C51 | VVV-J181952.92-292447.2 | 13 575 224 000 906 | 16.20 ± 0.32 | 32.1 | 0–2170 | 0.00017 | Early-type galaxy |
| C52 | VVV-J182027.00-321931.1 | 13 849 658 000 489 | 15.63 ± 0.20 | 15.6 | 1000–2550 | 0.00013 | Early-type galaxy |
| C52 | VVV-J182052.11-322058.3 | 13 853 755 001 577 | 15.99 ± 0.17 | 13.0 | 1000–2550 | 0.00011 | Early-type galaxy |
| C53 | VVV-J182807.31-325038.0 | 13 898 832 000 212 | 16.00 ± 0.23 | 21.7 | 1000–2550 | 0.00016 | Early-type galaxy |
| C53 | VVV-J182809.51-325239.3 | 13 902 928 000 442 | 17.04 ± 0.22 | 16.5 | 1000–2550 | 0.00020 | Late-type galaxy |
| C53 | VVV-J182809.69-324820.6 | 13 894 736 002 365 | 16.81 ± 0.22 | 17.4 | 1000–2550 | 0.00019 | Early-type galaxy |
| C53 | VVV-J182826.63-325145.4 | 13 898 833 000 294 | 16.54 ± 0.21 | 14.9 | 1000–2550 | 0.00014 | Late-type galaxy |
| C53 | VVV-J182834.03-325437.9 | 13 907 025 000 679 | 16.28 ± 0.19 | 15.0 | 1000–2550 | 0.00011 | Early-type galaxy |

*Fermi*-LAT sources lying at higher interstellar extinction regions, we did not find any NIR nor MIR candidates.

Considering that some UGS have multiple candidates, it is crucial to establish criteria for prioritising the selection of the objects for follow-up observations. This selection process is based on additional criteria that includes magnitude, distance to the *Fermi* source, variability, interstellar extinction and visual inspection. As a result, the priority candidate for the *Fermi*-LAT source A9 is VVV-J175851.46-411016.0, which is the brightest, closest, the most variable source and lowest interstellar extinction. For the *Fermi*-LAT source A12, the priority candidate is VVV-J181258.71-314346.7, using the same criteria mentioned above. Within the C subsample, the priority candidates are VVV-J180826.32-352214.7 for C44, VVV-J181440.95-341915.4 for C48, VVV-J181751.39-333117.3 for C50, VVV-J182052.11-322058.3 for C52, and VVV-J182807.31-325038.0 for C53.

## 4 SUMMARY

In this work we present criteria for selecting AGN candidates as counterparts to *Fermi*-LAT sources, based on NIR and MIR photometry from the VVV and WISE surveys. We analysed a sample of 78 high-energy $\gamma$-ray sources located at low Galactic latitudes without any previous source associations at any wavelength and lying in the footprint of the VVV survey. To start with, we divided the sample in three subsamples, considering the interstellar extinctions and semimajor axis of the *Fermi*-LAT uncertainties.

We analysed photometric data from the VVV and WISE surveys, following the methodology reported by Pichel et al. (2020) to search for blazars and Baravalle et al. (2023) to identify AGN candidates. The following colour cuts were used to identify VVV AGN candidates associated to the UGS sample in the near-IR data: $0.5 < (J\text{–}K_s) < 2.5$ mag; $0.5 < (H\text{–}K_s) < 2.0$ mag; $0.4 < (J\text{–}H) < 2.0$ mag and $0.2 < (Y\text{–}J) < 2.0$ mag. These sources are located in specific regions in the NIR CCD, clearly separated from stars and other extragalactic sources. Upon visual inspection, we removed the contaminated sources such as those with nearby bright stars or stellar associations.

We then selected 27 VVV AGN candidates within 14 *Fermi*-LAT positional uncertainties ellipses using the VVV survey. These objects satisfy the colour cuts and also visually look as a galaxy or have point-like morphology. We have also explored the light curves of all sources reported in Table 4 and applied the fractional variability amplitude and the slope of variation in the $K_s$ passband. In general, most of the candidates show variability $\sigma_{rms} > 12$ and slopes in agreement with the limits defined by Cioni et al. (2011). These results suggest the presence of type-1 AGN. However, there are four objects with low variability $\sigma_{rms} < 8.0$ and smaller slopes that might not be ruled out. We also found 2 blazar candidates in the regions of 2 *Fermi*-LAT sources using WISE data. There is no match between VVV and WISE candidates.

The combination of $YJHK_s$ colours and $K_s$ variability criteria have been useful for AGN selection, including its use in identifying counterparts to *Fermi*-LAT $\gamma$-ray sources. Finally, we aim to perform NIR spectroscopic observations to confirm the extragalactic nature of

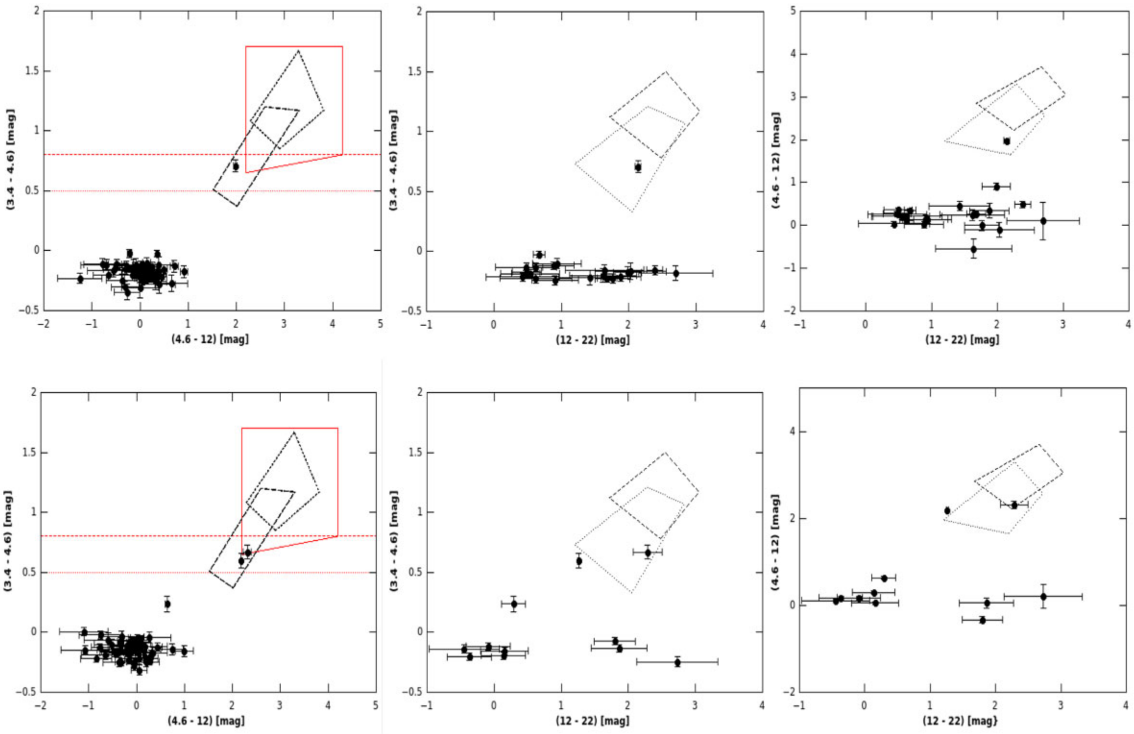


**Figure 19.** Mid-IR CCD for the *Fermi*-LAT sources A8 (top) and B10 (bottom) using WISE data (black dots). The two blazar classes of BZB (BL Lac) and BZQ (FSRQ) are shown in dash- and dot- black lines, respectively. The dotted and dashed red horizontal lines represent the limits for AGN from Stern et al. (2012) and Assef et al. (2018), respectively. The solid red box denotes the defined region of QSO/AGN from Jarrett et al. (2011).

the AGN candidates reported here. Particularly useful would be the data provided by Vera C. Rubin Observatory Legacy Survey of Space and Time (LSST Science Collaboration et al. 2009) and the eROSITA X-ray telescope (Brunner et al. 2022) in order to complement this study.

## ACKNOWLEDGEMENTS

We want to thank the referee for useful comments and suggestions which has helped to improve this paper. This work was partially supported by Consejo de Investigaciones Científicas y Técnicas (CONICET), Secretaría de Ciencia y Técnica de la Universidad Nacional de Córdoba (SecyT), and Secretaría de Ciencia y Técnica de la Universidad Nacional de San Juan. DM gratefully acknowledges support from the ANID BASAL projects ACE210002 and FB210003, from Fondecyt Project No. 1220724, and from CNPq/Brazil Project 350104/2022-0. The authors gratefully acknowledge data from the ESO Public Survey program IDs 179.B-2002 and 198.B-2004 taken with the VISTA telescope, and products from the Cambridge Astronomical Survey Unit (CASU). We also thank Román Vena Valdarenas for helping us to improve the figures. This research has made use of the VizieR catalogue access tool, CDS, Strasbourg, France (DOI: 10.26093/cds/vizier). The original description of the VizieR service was published in 2000, A&AS 143, 23.

## 5 DATA AVAILABILITY

The data underlying this article are available in https://vvvsurvey.org/ and https://www.nasa.gov/mission/⟨0:italic ⟩WISE⟨/0:italic⟩.

## REFERENCES

Abdollahi S. et al., 2020, ApJS, 247, 33
Acero F., Ackermann M., 2015, ApJS, 218, 23
Ackermann M. et al., 2012, ApJ, 753, L83
Amôres E. B. et al., 2012, AJ, 144, 127
Antonucci R., 1993, ARA&A, 31, 473
Assef R. J. et al., 2010, ApJ, 713, L970
Assef R. J., Stern D., Noirot G., Jun H. D., Cutri R. M., Eisenhardt P. R. M., 2018, ApJS, 234, 23
Atwood W. B., 2009, ApJ, 697, L1071
Baravalle L. D., Alonso M. V., Nilo Castellón J. L., Beamín J. C., Minniti D., 2018, AJ., 155, 46
Baravalle L. D. et al., 2019, ApJ, 874, L46
Baravalle L. D. et al., 2021, MNRAS, 502, 601
Baravalle L. D. et al., 2023, MNRAS, 520, 5950
Bertin E., 2011, in Evans I. N., Accomazzi A., Mink D. J., Rots A. H.eds, Astronomical Data Analysis Software and Systems XX vol. 442, Astronomical Society of the Pacific, San Francisco, , Astronomical Society of the Pacific Conference Series, 435
Brunner H. et al., 2022, A&A, 661, 1
Catelan M. et al., 2011, in McWilliam A.ed., Proceedings of the International Society for Optical, RR Lyrae Stars, Metal-Poor Stars, and the Galaxy vol. 5, 145
Chen P. S., Fu H. W., Gao Y. F., 2005, New A, 11, 27
Cheung C. C., Donato D., Gehrels N., Sokolovsky K. V., Giroletti M., 2012, ApJ, 756, L33
Cioni M.-R. et al., 2011, The Messenger, 144, 25
Cioni M.-R. L. et al., 2013, A&A, 549, 29
Coldwell G., Alonso S., Duplancic F., Hempel M., Ivanov V. D., Minniti D., 2014, A&A, 569, 49
D'Abrusco R., Massaro F., Ajello M., Grindlay J. E., Smith H. A., Tosti G., 2012, ApJ, 748, L68
D'Abrusco R., Massaro F., Paggi A., Masetti N., Tosti G., Giroletti M., Smith H. A., 2013, ApJS, 206, 12

D'Abrusco R., Massaro F., Paggi A., Smith H. A., Masetti N., Landoni M., Tosti G., 2014, ApJS, 215, 14
D'Abrusco R. et al., 2019, ApJS, 242, 4
Daza-Perilla I. V. et al., 2023, MNRAS, 524, 678
Doert M., Errando M., 2014, ApJ, 782, L41
Donoso L., 2020, PhD thesis, Universidad Nacional de Córdoba, Argentina
Edelson R., Malkan M., 2012, ApJ, 751, L52
Edelson R., Turner T. J., Pounds K., Vaughan S., Markowitz A., Marshall H., Dobbie P., Warwick R., 2002, ApJ, 568, L610
Emerson J., McPherson A., Sutherland W., 2006, The Messenger, 126, 41
Fu Y., Wu X.-B., Yang Q., Brown A. G. A., Feng X., Ma Q., Li S., 2021, ApJS, 254, 6
Fu Y. et al., 2022, ApJS, 261, 32
Galdeano D. et al., 2021, A&A, 646, 146
García-Pérez A. et al., 2023, AJ, 165, 127
Hassan T., Mirabal N., Contreras J. L., Oya I., 2013, MNRAS, 428, 220
Hovatta T. et al., 2014, AJ, 147, 143
Husemann B. et al., 2022, A&A, 659, 124
Ilić D. et al., 2017, Frontiers in Astronomy and Space Sciences, 4, 12
Jarrett T. H. et al., 2011, ApJ, 735, L112
Kraan-Korteweg R. C., 2000, A&AS, 141, 123
LSST Science Collaboration et al., 2009, preprint (arXiv:0912.0201)
Lefaucheur J., Pita S., 2017, A&A, 602, 86
León-Tavares J., Valtaoja E., Giommi P., Polenta G., Tornikoski M., Lähteenmäki A., Gasparrini D., Cutini S., 2012, ApJ, 754, L23
Li D., Starling R. L. C., Saxton R. D., Pan H.-W., Yuan W., 2022, MNRAS, 512, 3858
López-Caniego M., González-Nuevo J., Massardi M., Bonavera L., Herranz D., Negrello M., 2013, MNRAS, 430, 1566
Maeda K. et al., 2011, ApJ, 729, L103
Mao L., Yi T., 2021, ApJS, 255, 10
Massaro F., D'Abrusco R., 2016, ApJ, 827, L67
Massaro E., Maselli A., Leto C., Marchegiani P., Perri M., Giommi P., Piranomonte S., 2015, Ap&SS, 357, 75
Minniti D. et al., 2010, New A, 15, 433
Molnar T. A., Sanders J. L., Smith L. C., Belokurov V., Lucas P., Minniti D., 2022, MNRAS, 509, 2566
Nandra K., George I. M., Mushotzky R. F., Turner T. J., Yaqoob T., 1997, ApJ, 476, L70
do Nascimento J. C. et al., 2019, MNRAS, 486, 5075
Netzer H., 2015, ARA&A, 53, 365
Padovani P. et al., 2017, A&A Rev., 25, 2
Paggi A. et al., 2014, AJ, 147, 112
Peña-Herazo H. A. et al., 2021, AJ, 162, 177
Pennock C. M. et al., 2022, MNRAS, 515, 6046
Pichel A. et al., 2020, MNRAS, 491, 3448
Raiteri C. M. et al., 2014, MNRAS, 442, 629
Rembold S. B. et al., 2017, MNRAS, 472, 4382
Richards G. T. et al., 2006, ApJS, 166, 470
Saito R. et al., 2010, The Messenger, 141, 24
Sandrinelli A., Covino S., Treves A., 2014, A&A, 562, 79
Schinzel F. K., Petrov L., Taylor G. B., Mahony E. K., Edwards P. G., Kovalev Y. Y., 2015, ApJS, 217, 4
Schlafly E. F., Finkbeiner D. P., 2011, AJ, 737, 103
Sevenster M. N., Chapman J. M., Habing H. J., Killeen N. E. B., Lindqvist M., 1997, A&AS, 122, 79
Shakura N. I., Sunyaev R. A., 1973, A&A, 24, 337
Skrutskie M. F. et al., 2006, AJ, 131, 1163
Smith L. C. et al., 2018, MNRAS, 474, 1826
Soto M. et al., 2022, MNRAS, 513, 2747
Stern D. et al., 2005, ApJ, 631, L163
Stern D. et al., 2012, ApJ, 753, L30
Stickel M., Padovani P., Urry C. M., Fried J. W., Kuehr H., 1991, ApJ, 374, L431
Stocke J. T., Morris S. L., Gioia I. M., Maccacaro T., Schild R., Wolter A., Fleming T. A., Henry J. P., 1991, ApJS, 76, 813
Thompson D. J., 2008, Rep. Prog. Phys., 71, 116901
Ulrich M.-H., Maraschi L., Urry C. M., 1997, ARA&A, 35, 445
Urry C. M., Padovani P., 1995, PASP, 107, 803
Véron-Cetty M. P., Véron P., 2010, A&A, 518, 10
Wright E. L. et al., 2010, AJ, 140, 1868

This paper has been typeset from a TEX/LATEX file prepared by the author.